# Acquiring real kinetics of reactions in inhibitory atmosphere containing product gases using micro fluidized bed

Xuejing Liu[a], Wenqian Hao[a], Kexin Wang[a], Yingche Wang[a], Ping An[a], Hong Zhang[a], Junrong Yue[b], Dingrong Bai[a]*, Guangwen Xu[a,b]*

[a] Institute of Industrial Chemistry and Energy Technology, Key Laboratory on Resources Chemicals and Materials of Ministry of Education, Shenyang University of Chemical Technology, Shenyang, 110142, China

[b] State Key Laboratory of Multi-phase Complex Systems, Institute of Process Engineering, Chinese Academy of Sciences, Beijing, 100190, China

* corresponding authors

E-mail address: drbai@icloud.com (D. Bai), gwxu@ipe.ac.cn (G. Xu).

**Abstract:**

The study proposed an isotopes-tagging method for investigation of reactions under the atmosphere of product gas. To illustrate this method, the calcination kinetics of calcium carbonate $Ca^{13}CO_3$ in $CO_2$ atmospheres were investigated by monitoring $^{13}CO_2$ produced using a micro fluidized bed reaction analyzer (MFBRA). The results demonstrated that the presence of $CO_2$ in the reaction atmosphere increases the apparent activation energy. The increase in the apparent activation energy is, however, significantly overestimated by the TGA because of the excessive suppression by stagnated product gas inside the sample crucible. Comparatively, the results from the MFBRA are due primarily to the thermal

equilibrium limitation, because the gas diffusion in the MFBRA is essentially eliminated. It is thus concluded that the MFBRA is quite capable of acquiring the real kinetics of reactions in such inhibitory atmospheres.

atmosphere.

**Key words:** micro fluidized bed, gas-solids reaction, kinetics, isotopes tagging, inhibitory atmosphere.

## 1. Introduction

Gas-solid reactions exist widely in the fields of chemistry, chemical engineering, metallurgy, environment, energy conversion, materials science and engineering, etc.[1] Accurately understanding the reaction kinetics and behavior has always been important for scientific research and technology development.

There are some gas-solid reactions taking place in inhibitory atmospheres containing product gases. For example, as an important gas-solid reaction encountered in some processes such as cement manufacturing, flue gas desulfurization, and chemical looping combustion, decomposition of calcium carbonate ($CaCO_3$) is actually accomplished in $CO_2$-containing atmospheres. As an advanced combustion technology, the calcium looping (CaL) process is based on cyclic CaO carbonation (i.e. CaO reacts with $CO_2$ to form $CaCO_3$) and calcium carbonate calcination (i.e. $CaCO_3$ decomposes to produce CaO and $CO_2$ in the presence of $CO_2$) reactions[2, 3]. In principle, the kinetics of calcination are affected by the presence of $CO_2$ in the atmosphere, which is, however, not yet fully understood although a few research have

been reported[4-8]. Khinast et al.[9] studied the limestone calcination behavior under different $CO_2/N_2$ mixtures by a exponentially with increasing $CO_2$ partial pressure. Garcia-Labiano et al.[10] reported that increasing $CO_2$ partial pressure decreased the calcination rate, which was more pronounced at higher $CO_2$ concentrations. However, it is worth noting that as reported by several researchers[11-15], the TGA, due to its stronger inhibition of diffusion and lower heat and mass transfer rates, may provide inaccurate information for those reactions occurring in the atmosphere of product gas, For example, under the 100% $CO_2$ environment, the apparent activation energy was obtained as unreasonably high as over 2000 kJ/mol, with the reaction to complete in several minutes[16], which does not match the reaction times reported in the literature for fluidized bed chemical looping experiments. Thus, a new approach is needed to acquire the correct kinetics of reactions inhibited by the product gas containing atmosphere, such as $CaCO_3$ decomposition in the presence of $CO_2$.

The micro fluidized bed reaction reactor (MFBRA) is a novel thermal analyzer, which was first proposed by Xu[17] in 2005, and has become commercially available after extensive research and developments[18-20]. In an MFBRA, a fluidized bed of millimeter diameters is employed as an isothermal differential reactor for the characterization of gas-solid reactions[21]. In comparison to TGA, MFBRA is advantageously featured by (1) high rates of heat and mass transfer, (2) capability of online instantaneously pulse feeding and super-fast heating of powder reactant to bed temperature, (3) negligible external diffusion inhibition, and (4) fast on-line measurement.[19, 20] Until now, it has been successfully applied to study the mechanisms and kinetics of a variety of gas-solid reactions, including pyrolysis[22-24], gasification[14, 25, 26],

combustion[27, 28] of coal, biomass, oil shale and chars, calcination[11, 20] and reduction[29-32] of various materials as well as catalytic gas-solid reactions[33, 34], etc. These applications have demonstrated that MFBRA is effective, reliable, and adaptable to various gas-solids reactions. Recently, new progress has been made to extend MFBRA's capability in thermal analysis, e.g. by integrating a micro-balance (i.e. FB-TGA) to be able to monitor the change of sample mass and gas products[35, 36], by heating the fluidized bed with an induction heater (i.e. IHFB-TGA)[36-38]. These novel reactor configurations greatly enhanced the reliability of micro fluidized bed reactors for complex feedstocks because of the use of larger amount of sample particles.

Using both MFBRA and TGA, Jiang et al.[11] characterized the calcination reaction of magnesite powder in nitrogen and air atmospheres. They found that the activation energy and reaction completion time obtained with TGA were significantly higher than those with MFBRA. It was believed that the difference might be attributable to the inhibition on the reaction by the produced $CO_2$ gas surrounding the sample particles, which would be remarkably higher inside the TGA crucible than in MFBRA. This is, however, not yet validated by direct experiments. When attempts were made to verify this through MFBRA experiments using fluidizing gas containing $CO_2$, difficulties arose as how to distinguish between a small amount of product gas $CO_2$ and a large amount of fluidized gas $CO_2$ because the MFBRA determines the reaction kinetics data based on the measured time-series of product gas species.

To identify the $CO_2$ gases produced by $CaCO_3$ calcination and introduced by the fluidizing

gas, we introduced the isotope-tagging method, which has been used in the investigation of heterogenous catalytic reactions[39, 40], to the gas-solid reaction using MFBRA. In this paper, the raw reactants are selected deliberately so that the isotopes contained in the gas products are different from those contained in the same gas component in the fluidizing gas. To consider a specific example to illustrate this method, calcinations of calcium carbonate in atmospheres of varying $CO_2$ content were conducted using $Ca^{13}CO_3$, rather than $CaCO_3$, as a reactant in this study. When $Ca^{13}CO_3$ was decomposed in MFBRA under atmospheres with different $CO_2$ concentrations, the $^{13}CO_2$ produced from calcination reaction was easily recognizable and analyzable because its isotope was different from $CO_2$ of fluidizing gas (i.e. $^{12}CO_2$). This study, for the first time, demonstrates a successful investigation of a gas-solid reaction in atmospheres containing product gas by the isotopes-tagging method. With this novel experimental method, the advantages of MFBRA for characterizations of gas-solid reactions are further demonstrated.

## 2. Experimental section

### 2.1 Experimental materials and methods

Analytical grade $CaCO_3$ (Sinopharm Chemical Reagent Company, China) and $Ca^{13}CO_3$ (Sigma Aldrich, America) were used as raw materials for the experiments (Note that if not specified, the carbon in $CaCO_3$ and $CO_2$ in this paper defaults to $^{12}C$). The samples were dried at 120 °C for 24h in an oven before the experiments. The mean particle size is about 80 μm for $Ca^{13}CO_3$ and 50 μm for $CaCO_3$ as measured by Beckman Coulter LS 13 320 Particle Size

Analyzer (America). Although the particle sizes were slightly different between $CaCO_3$ and $Ca^{13}CO_3$, the difference in terms of decomposition behavior between them is negligible. Therefore, the $CaCO_3$ sample can be replaced by $Ca^{13}CO_3$ sample for tests in MFBRA.

The decomposition of $Ca^{13}CO_3$ experiments was carried out at atmospheric pressure in the MFBRA. Figure 1 shows a general schematic process diagram of the MFBRA, which was acquired from China Energy Clean Innovation Corporation. The MFBRA mainly consists of four parts: (1) an electric furnace, (2) a sample pulse feeding system, (3) a micro fluidized bed reactor often made of quartz glass with a diameter of 20 mm, and (4) an online process mass spectrometry (MS). Prior to each experiment, the quartz sand (3 g, particle size of 150~270 μm) was loaded in the MFB reactor as the bed material. The MFB reactor was heated to the preset temperature in the range of 700-1100°C with an interval of 50°C. When the preset temperature was reached, the fluidizing gas mixture having $CO_2$ concentration from 0% to 100% $CO_2$ in $N_2$, was introduced into the MFB reactor. The $CO_2$ and $N_2$ gases were measured and controlled by electronic mass flow controllers. The total fluidizing gas flow rate was about 300 mL/min (under the standard temperature and pressure). When the stable fluidization was attained, the test sample of approximately 15 mg was rapidly injected into the MFB reactor by a pressurized gas pulse. During the experiments, both the quartz sand and sample particles were under the stable fluidization state. The generated gas product $^{13}CO_2$ was analyzed and recorded online by the MS (Ametek, Dycorsystem 2000).

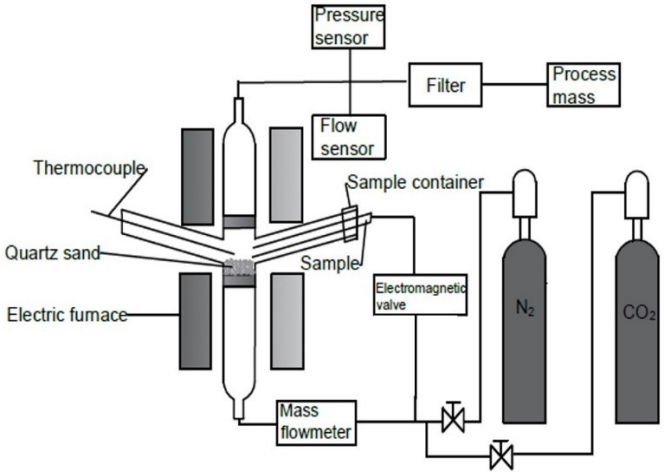


Figure 1. A schematic diagram of MFBRA.

In order to show that $CO_2$ and $^{13}CO_2$ can be distinguished by the MS, the decomposition experiments of $Ca^{13}CO_3$ mixed with $CaCO_3$ were carried out at 700°C in the atmosphere of $N_2$ in the MFBRA. As shown in Figure 2, it is obvious that both $CO_2$ and $^{13}CO_2$ can be separately detected by MS, indicating that the use of isotope-tagging approach to differentiate the product gas is feasible.

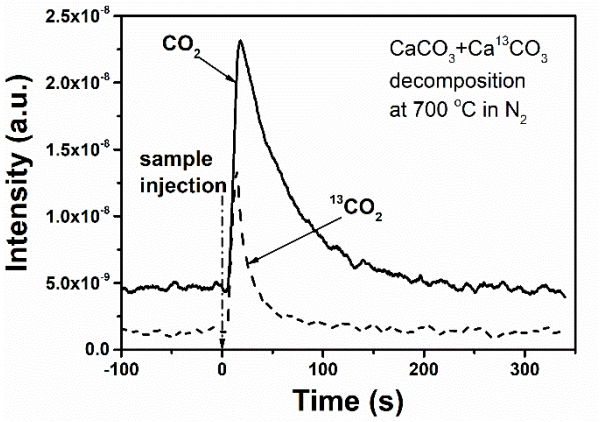


Figure 2. $CO_2$ and $^{13}CO_2$ release curves from decomposition of $CaCO_3$ and $Ca^{13}CO_3$ mixture in MFBRA at 700 °C in the atmosphere of $N_2$.

For comparison purpose, non-isothermal calcination tests of $CaCO_3$ were also performed in a TGA (TG-DTA8121, Rigaku, Japan) by raising the temperature from room temperature to

1100 °C at heating rates of 3, 5, 7, 10, 15, 20 and 40 °C/min in the atmospheres of $CO_2/N_2$ with volumetric $CO_2$ contents of 0%, 1%, 10%, 30%, 60% and 100%, respectively. During the TGA tests, the sample amount, the crucible ($Al_2O_3$) height and flow rate of gas through the cell chamber were 10.5±0.5 mg, 2.5 mm and 200 mL/min, respectively. A test was judged to be complete when the sample weight became constant.

**2.2 Data Analysis Methods**

For the TGA tests, the conversion $x$ was calculated based on the mass loss data as shown below

$$x=\frac{w_0-w_i}{w_o-w_{ash}} \quad x = \frac{w_0-w_i}{w_o-w_{ash}}. \tag{1}$$

where $w_o$ is the initial sample mass, $w_i$ is the sample mass at time $t_i$, and $w_{ash}$ is the remaining mass of the sample after completion of the calcination test.

For non-isothermal reactions, the so-called combination heating rate method is typically employed for determination of reaction kinetics. The method considers all the thermal analysis curves obtained at various heating rates to obtain averaged kinetic parameters. Among many such methods proposed in the literature[41-43], the Flynn-Wall-Ozawa (FWO) method[41] has been widely used, which can be described as follows

$$lg\,\beta=lg\left[AE/RG(x)\right]-2.315-0.4567\,E/RT$$

$$lg\,\beta = lg[AE/RG(x)] - 2.315 - 0.4567\,E/RT. \tag{2}$$

where $\beta$ is the heating rate; $A$ is the pre-exponential factor, $s^{-1}$; $E$ is the activation energy,

J/mol; $T$ is the reaction temperature, $K$; and $G(x)$ is the integral reaction model function. As shown in Eq. (2), the FWO equation yields an activation energy $E$ for each given conversion $x$ under which $G(x)$ is a constant. Therefore, for each value of $x$, $lg\ \beta$ can be plotted against $1/T$ to yield a straight line that has a slope of $0.4567E/R$, based on which the value of activation energy, $E$, can be calculated. Then, the apparent activation energy of the reaction can be determined through extrapolating the correlation curve of $E$ vs. $x$ to $x$=0. The FWO approach, as a typical model free method, obtains the activation energy without need of pre-selecting a reaction model, but the pre-exponential factor cannot be estimated directly. Therefore, the Coats-Redfern approach[42] was adopted to determine the reaction mechanism model that can best describe the reaction. The Coats-Redfern equation can be expressed as follows

$$\ln(G(x)/T^2) = \ln(AR/\beta E) - E/RT \qquad \ln\left[G(x)/T^2\right] = \ln(AR/\beta E) - E/RT \cdot \tag{3}$$

The activation energies at different heating rates can be calculated by substituting different a mechanism model function into the Eq. (3) that yields the best linear fitting between $ln\ [G(x)/T^2]$ and $1/T$. The apparent activation energy can be obtained through extrapolating the activation energies obtained at different heating rates to the zero-heating rate (i.e. $\beta \rightarrow 0$). Then, the function $G(x)$, which yields an apparent activation energy that is closest to that obtained from the FWO equation, can be considered as the most appropriate reaction mechanism. As a result, the pre-exponential factor $A$ can be determined based on the reaction mechanism function model.

Due to small amount of sample and fast heating rate, the bed temperature change caused by sample injection is negligible, and the reaction in the MFBRA can be reasonably

considered to be isothermal. Under isothermal conditions, the reaction rate can be described in the form of

$$dx/dt = k(T)f(x) = A\exp(-E/RT)f(x). \quad (4)$$

Taking natural logarithm on both sides of Eq. (4) obtains

$$\ln(dx/dt) ¿ -E/RT + \ln A + \ln f(x). \quad (5)$$

where *k(T)* and *f(x)* represent reaction rate constant defined by the Arrhenius Equation ( $k(T) = A\exp(-E/RT)$ $k(T) = A\,exp(-E/RT)$) and reaction mechanism function, respectively. Since temperature $T$ is constant under isothermal conditions, so does the reaction rate constant *k(T)*, which allows the mechanism function *f(x)* to be separated. Therefore, the apparent activation energy can be determined by plotting *ln(dx/dt)* versus *1/T* at any given conversion *x* (under which the mechanism function *f(x)* is a constant).

Under isothermal conditions, the mechanism model function is simply deduced to the following equation

$$G(x) = k(T) \times t. \quad (6)$$

Based on Eq. (6), the reaction rate constant *k(T)* can be obtained for each temperature from the linear regression of *G(x)* versus *t*. Then, the activation energy *E* and pre-exponential factor *A* can be obtained based on Arrhenius Equation. Again, the *G(x)* that best fits the experimental data is taken as the reaction function model.

## 3. Results and Discussion

### 3.1 Non-Isothermal Tests in TGA

The experiments of $CaCO_3$ decomposition were first performed in TGA with programmed heating in the atmosphere of $N_2/CO_2$ with different $CO_2$ concentrations varying from 0% to 100%. Figure 3 shows the results of conversion as a function of temperature in TGA at different heating rates in $N_2$ with 0% $CO_2$ and 100% $CO_2$. As shown in the figure, the temperature corresponding to the same conversion gradually increase with increasing heating rate. The effect of heating rate is more pronounced for 0% $CO_2$ than for 100% $CO_2$. The reason is that the inhibition effect of $CO_2$ on the $CaCO_3$ decomposition becomes more and more dominant with the increase of $CO_2$ concentration.

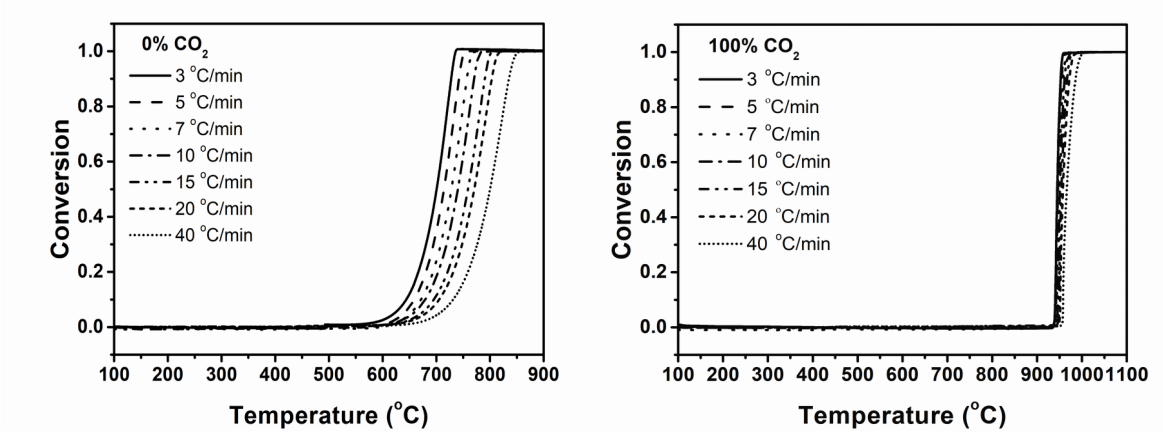


Figure 3. Variation of conversion with temperature measured in TGA at different heating rates in the atmospheres of 0% (left) and 100% $CO_2$ (right).

For a constant conversion value of $x$, $lg\,\beta \sim 1/T$ is a straight line, as shown in Figure 4. The correlation coefficients of all fitting lines are above 0.99, suggesting that linear regressions are quite satisfactory. The values of activation energy derived from the slopes of the fitting lines in Figure 4 are plotted in Figure 5 as a function of the conversion $x$. The lines in Figure 5 are polynomial fits between the apparent activation energy $E$ and the conversion $x$ with correlation coefficients $R^2$ greater than 0.996. Extrapolating the fitted curves to conversion

*x=0* obtains $E_{x\to 0}$ of 240.6 kJ/mol in 0% of $CO_2$ and 2047.2 kJ/mol in 100% $CO_2$. These results are comparable with those reported in the literature[16, 44]. According to the FWO approach, the $E_{x\to 0}$ represents the apparent activation energy to initiate the $CaCO_3$ decomposition to produce the products of CaO and $CO_2$.

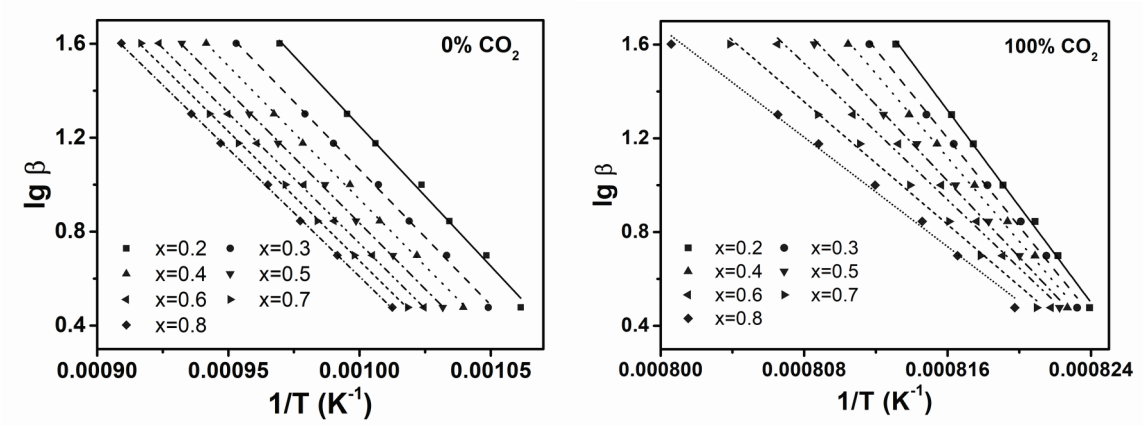


Figure 4. Relationship of *lgβ* with *1/T* for calcination of $CaCO_3$ power from tests in TGA in the atmosphere of $N_2$ with 0% $CO_2$ and 100% $CO_2$.

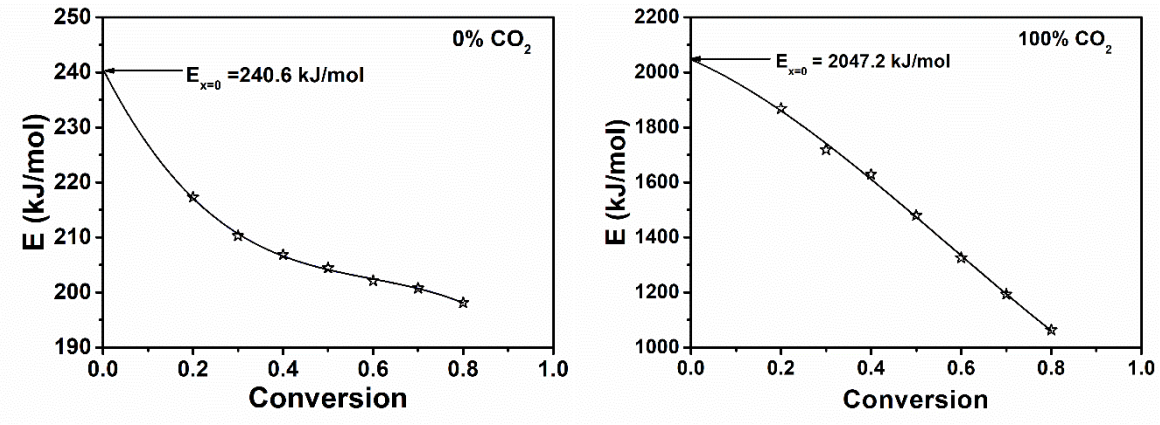


Figure 5 Correlation of activation energy *E* and conversion derived from the data in Figure 5 in the atmosphere of $N_2$ with 0% $CO_2$ and 100% $CO_2$.

Based on the same approach, the activation energies of the $CaCO_3$ decomposition under the atmospheres containing 1%, 10%, 30% and 60% $CO_2$ are estimated. The variation of the apparent activation energy *E* with $CO_2$ concentration is shown in Figure 6. It is observed that the activation energy increases exponentially with increasing $CO_2$ concentration, and the

relationship can be best presented by an empirical correlation as following

$$E=817.2\,e^{\frac{-C_{CO_2}}{2.3}}-1144.03\,e^{\frac{-C_{CO_2}}{48.3}}+2200.8 \qquad E = 817.22e^{-\frac{c_{CO_2}}{2.31}} - 1144.03e^{-\frac{c_{CO_2}}{48.31}} + 2200.79 \quad (7)$$

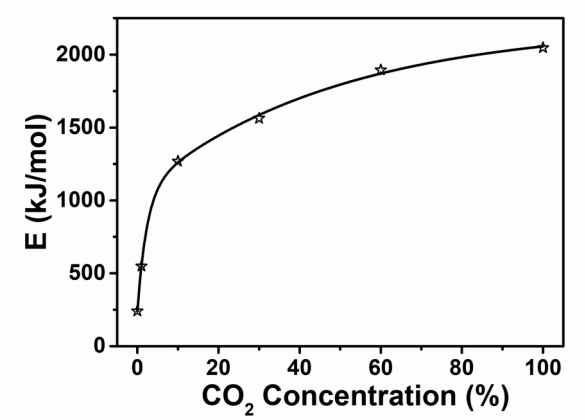


Figure 6. Relationship of the activation energy $E$ with $CO_2$ concentration for $CaCO_3$ decomposition in TGA.

To identify the reaction mechanism, the four reaction function models that are normally applicable to gas-solid reactions[45] were submitted into Eq. (3) of the Coats-Redfern equation. The estimated activation energies for the heating rates of 5, 7 and 10 °C/min are summarized in Table 1. Based on these data, $E_{\beta\rightarrow 0}$ can be obtained by extrapolation. From Table 1, it is seen that the all four mechanism function models fit the experimental mathematically well, but the resulting activation energies are significantly different. Therefore, the best reaction model needs to be identified by comparing $E$ value at $\beta\rightarrow 0$ with that calculated by the FWO equation. Under $N_2$ environment, the activation energy is obtained as 240.6 kJ/mol by the FWO method, which is clearly best matched by the shrinking core model (cylinder) $G(x)= 1-(1-x)^{1/2}$ with an activation energy of 235.1 kJ/mol. Under 100% $CO_2$ environment the nucleation and growth control model (n=1.5) $G(x)=[-ln(1-x)]^{2/3}$ yields an activation energy of

2081.6 kJ/mol, approximately the same as that obtained from FWO method (2047.2 kJ/mol). Therefore, the shrinking core model and the nucleation and growth control model can be considered to be the suitable mechanism function models in the atmospheres containing 0% and 100% $CO_2$, respectively. Consequently, based on the Coats-Redfern equation the pre-exponential factors in the atmospheres of 0% $CO_2$ and 100% $CO_2$ can be determined as $1.4\times10^8$ and $2.3\times10^{81}$ $s^{-1}$, respectively.

Table1 Fitting results using the Coats-Redfern formula for literature-reported mechanism models based on TGA data in $N_2$ and $CO_2$.

| | G(x) expressions | β→0 °C/min | β=5 °C/min | | β=7 °C/min | | β=10 °C/min | |
|---|---|---|---|---|---|---|---|---|
| | | E (kJ/mol) | E (kJ/mol) | r | E (kJ/mol) | r | E (kJ/mol) | r |
| 0% $CO_2$ | $[-\ln(1-x)]^{1/2}$ | 132.5 | 126.7 | 0.994 | 126.3 | 0.993 | 122.6 | 0.994 |
| | $[-\ln(1-x)]^{2/3}$ | 182.4 | 174.4 | 0.994 | 173.9 | 0.994 | 169.1 | 0.994 |
| | **$1-(1-x)^{1/2}$** | **235.1** | **225.2** | **1** | **224.6** | **1** | **218.6** | **1** |
| | $1-(1-x)^{1/3}$ | 249.8 | 239.3 | 0.999 | 238.7 | 0.998 | 232.3 | 0.999 |
| 100% $CO_2$ | $[-\ln(1-x)]^{1/2}$ | 1556.2 | 1292.6 | 0.990 | 1183.9 | 0.990 | 1132.9 | 0.991 |
| | **$[-\ln(1-x)]^{2/3}$** | **2081.6** | **1730.3** | **0.990** | **1585.3** | **0.990** | **1517.4** | **0.991** |
| | $1-(1-x)^{1/2}$ | 2640.1 | 2188.2 | 0.974 | 2004.8 | 0.973 | 1915.7 | 0.975 |
| | $1-(1-x)^{1/3}$ | 2795.9 | 2320.2 | 0.976 | 2126.1 | 0.974 | 2032.9 | 0.976 |

### 3.2 Isothermal Tests in MFBRA

Figure 7 depicts variations of the measured $Ca^{13}CO_3$ conversion with time in MFBRA at

different temperatures in the atmosphere of 100% $CO_2$. Compared with the data measured in TGA at 40 °C/min (end temperature 1100°C), which is included in Figure 7 for the purpose of comparison, it shows that the conversion increases fast with time in the initial stage of decomposition and then gradually increases until the decomposition is completed in MFBRA. This reveals the great difference between TGA and MFBRA in characterizing reactions.

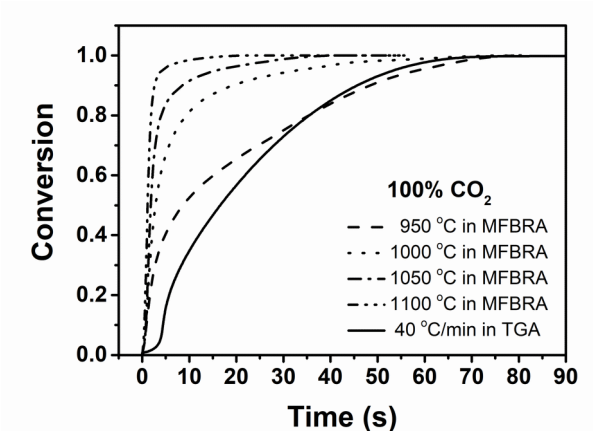


Figure 7. Variation of conversion with time for $Ca^{13}CO_3$ decomposition at different preset temperatures in 100% $CO_2$ in MFBRA and in TGA at 40 °C/min (end temperature 1100°C).

The variation of reaction rate with conversion is shown in Figure 8. At a given temperature, the reaction rate increases rapidly soon after the reaction is initiated, and reaches a maximum as the conversion further increases to around 0.2 to 0.4 depending on reaction temperature. As the reaction advances further the reaction rate starts to decline continuously. As the reaction temperature increases, the conversion corresponding to the maximum reaction rate also increases. At 900°C, the maximum reaction rate in $N_2$ reaches 0.3, while in 100% $CO_2$ at even a higher temperature (950°C), this value is only about 0.13. This again proves that $CO_2$ inhibits the decomposition reaction seriously.

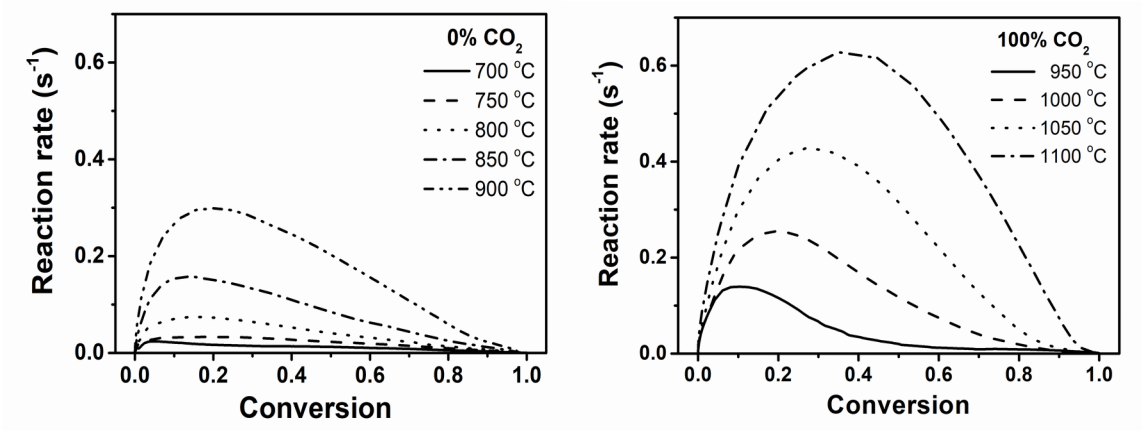


Figure 8. Reaction rate (*dx/dt*) varying with conversion for $Ca^{13}CO_3$ decomposition at different temperatures in the atmosphere of $N_2$ and $CO_2$ in MFBRA.

For conversions of 0.2, 0.3, 0.4, 0.5, 0.6, 0.7 and 0.8, the data of *ln(dx/dt)* are plotted against *1/T* in Figure 9. The correlation coefficients for all of the straight lines are above 0.99, indicating satisfactory regressions. According to Eq. (5), the activation energy values can be determined by the slopes of these straight lines, and the results are listed in Table 2. Based on these data, the average values of activation energy are calculated as 127.7 kJ/mol in $N_2$ without $CO_2$, and 271.5 kJ/mol in 100% $CO_2$ atmosphere, respectively.

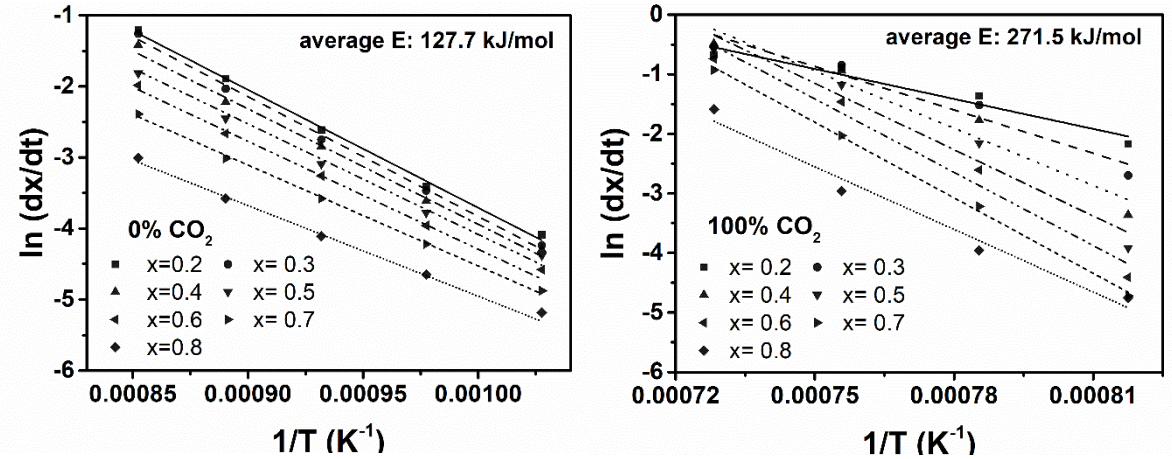


Figure 9. Fitting curves of *ln(dx/dt)* versus *1/T* for $Ca^{13}CO_3$ decomposition under the atmosphere of $N_2$ and $CO_2$ in MFBRA.

Table 2 the activation energy values determined by the slopes of the straight lines in Figure 10 according to Eq. (5) at different conversions.

| Conversion | 0.2 | 0.3 | 0.4 | 0.5 | 0.6 | 0.7 | 0.8 | Average E (kJ/mol) |
|---|---|---|---|---|---|---|---|---|
| | E (kJ/mol) | | | | | | | |
| 0% $CO_2$ | 138.0 | 140.1 | 135.3 | 129.5 | 126.4 | 118.2 | 106.2 | **127.7** |
| 100% $CO_2$ | 139.4 | 202.0 | 266.5 | 308.4 | 341.3 | 351.5 | 291.6 | **271.5** |

Similarly, the activation energies of $Ca^{13}CO_3$ decomposition in the atmospheres of 1%, 10%, 30% and 60% $CO_2$ are also calculated. The variation of apparent activation energy with $CO_2$ concentration is presented in Figure 10. The relationship between the activation energy and increasing $CO_2$ concentration can be best presented by an empirical correlation as following

$$E = -39.1\, e^{\frac{-C_{CO_2}}{1.5}} + 235.29\, e^{\frac{C_{CO_2}}{271.5}} - 68.6 \qquad E = -39.07e^{-\frac{C_{CO_2}}{1.46}} + 235.29e^{\frac{C_{CO_2}}{271.48}} - 68.55 \quad (8)$$

To determine the reaction mechanism, the four possible mechanism models of $CaCO_3$ calcination reported in the literature[45] are used to fit the experimental data obtained from MFBRA. The calculated activation energy and pre-exponential factors corresponding to these four reaction models are shown in Table 3. It shows that the shrinking core model (sphere) $G(x)= 1-(1-x)^{1/3}$ is the most suitable mechanism function model in the atmosphere of $N_2$ and $CO_2$ as it provides the highest fitting correlation in $CO_2$ environment and satisfactory regression in $N_2$.

Table 3 Activation energy of $Ca^{13}CO_3$ calcination reaction obtained with four reaction models using MFBRA-measured data in $N_2$ and $CO_2$ atmospheres.

| G(x) | 0% $CO_2$ | | | 100% $CO_2$ | | |
|---|---|---|---|---|---|---|
| | E (kJ/mol) | lg A ($s^{-1}$) | $R^2$ | E (kJ/mol) | lg A ($s^{-1}$) | $R^2$ |
| $[-\ln(1-x)]^{1/2}$ | 131.2 | 5.14 | 0.980 | 341.0 | 12.98 | 0.819 |
| $[-\ln(1-x)]^{2/3}$ | 130.9 | 5.24 | 0.985 | 332.2 | 12.71 | 0.873 |
| $1-(1-x)^{1/2}$ | 134.7 | 5.08 | 0.983 | 186.4 | 6.69 | 0.996 |
| **$1-(1-x)^{1/3}$** | **128.4** | **4.63** | **0.969** | **274.1** | **9.97** | **0.930** |

### 3.3 Comparison between TGA and MFBRA

#### 3.3.1 The activation energy

For the purpose of comparison, the relationship of activation energy with $CO_2$ concentration obtained from TGA and MFBRA tests are plotted in the Figure 10. It is apparent that for both MFBRA and TGA tests the apparent activation energy increases with increasing $CO_2$ concentration, but the increase in the activation energy is noticeably faster for TGA than for MFBRA. In terms of the ratio of the activation energy obtained from TGA to that obtained from MFBRA, it changes from 1.9 in $N_2$ to 3.7 when there is only 1% $CO_2$ in the atmosphere. Further increasing $CO_2$ in the atmosphere, the ratio of $E_{TGA}/E_{MFBRA}$ increases up to as high as 5 to 8. The results indicate that as $CO_2$ concentration in atmosphere increases, the product gas diffusion from TGA sample to surrounding atmosphere is suppressed more seriously. At 100% $CO_2$, the activation energy obtained by TGA is 2047.2 kJ/mol, a value that is apparently too high to be considered reasonable. In comparison, the MFBRA provides the reaction activation energy of 271.5 kJ/mol, more in line with the expectations. For MFBRA, however, the moderate increase in the activation energy with increasing $CO_2$ concentration is mainly due to the thermal equilibrium impact, which is confirmed in the next section.

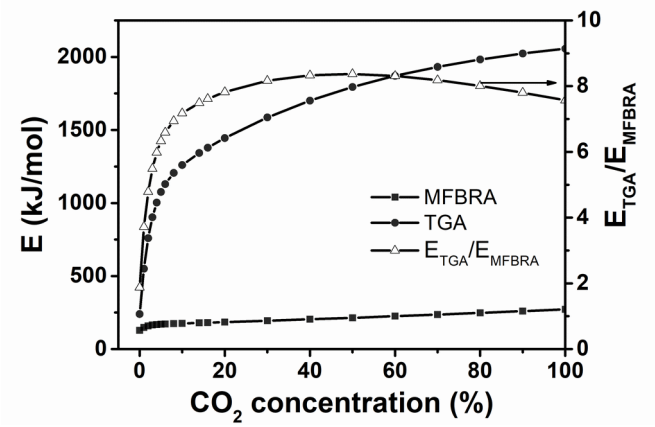


Figure 10. Relationship of activation energy with $CO_2$ concentration for $CaCO_3$ decomposition in MFBRA and in TGA.

### 3.3.2 The initial decomposition temperature

The initial temperatures of $CaCO_3$ decomposition with different $CO_2$ concentrations were obtained by both TGA and MFBRA, and the results are shown in Figure 11. During the experiments, the heating rate was 20 °C/min for TGA and MFBRA. For better understanding the influence of $CO_2$ atmospheres on $CaCO_3$ decomposition, the process simulations by Aspen Plus were also conducted, in which the RGibbs model was employed as the reactor to simulate decomposition process. For Aspen Plus simulations, the molar ratio of feeding gas and calcium carbonate was 9. The $CO_2$ concentrations in feeding gas with a mixture of $N_2$ and $CO_2$ were determined as 0 vol.%, 1 vol.%, 10 vol.%, 30 vol.%, 60 vol.% and 100 vol.%, respectively. All these parameter settings were consistent with those used in the experiments. The simulation results are also provided in Figure 11.

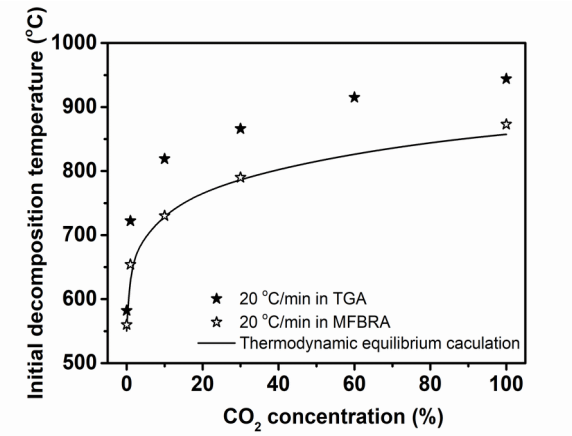


Figure 11. The initial temperature of $CaCO_3$ decomposition with different $N_2/CO_2$ mixtures at the heating rate of 20 °C/min in TGA, MFBRA and in the condition of thermodynamic equilibrium.

Figure 11 shows clearly that the initial temperature of $CaCO_3$ decomposition becomes higher and higher and increases exponentially with the increase of $CO_2$ concentration. For TGA, the initial decomposition temperature is about 580 °C under pure $N_2$ atmosphere, and increases sharply to 720 °C in the presence of only 1% $CO_2$ and to 935 °C under 100% $CO_2$. In comparison, the initial temperatures of $CaCO_3$ decomposition obtained by MFBRA are always lower than those obtained by TGA. The difference between MFBRA and TGA is about 30 °C at 0% $CO_2$, and increases to approximately 100 °C at ≥10% $CO_2$. Between MFBRA and thermal equilibrium calculations, the initial temperatures of $CaCO_3$ decomposition are very close, indicating that MFBRA is indeed approaching to the real reaction kinetics in the product gas strongly inhibited atmospheres. Therefore, for characterizing gas-solid reactions MFBRA is clearly superior than TGA because of its effective suppression of gas diffusion.

### 3.3.3 Reaction mechanism model

To further compare the data obtained in MFBRA and TGA, all results measured in $N_2$ with different $CO_2$ concentration are listed in Table 4. It shows that for both the TGA and MFBRA

the activation energy increases exponentially with increasing $CO_2$ concentration, but the reaction models and pre-exponential factors are very different.

Table 4 Kinetic parameters of $CaCO_3$ and $Ca^{13}CO_3$ calcination measured using TGA and MFBRA in $N_2$ with different $CO_2$ concentrations.

| $CO_2$ concentration | TGA | | | MFBRA | | |
|---|---|---|---|---|---|---|
| | E (kJ/mol) | A ($s^{-1}$) | G(x) | E (kJ/mol) | A ($s^{-1}$) | G(x) |
| 0% | 240.6 | $1.4\times10^{8}$ | $1-(1-x)^{1/2}$ | 127.7 | $4.3\times10^{4}$ | $1-(1-x)^{1/3}$ |
| 1% | 548.4 | $2.5\times10^{22}$ | $[-\ln(1-x)]^{2/3}$ | 148.0 | $7.5\times10^{5}$ | $1-(1-x)^{1/2}$ |
| 10% | 1268.8 | $1.8\times10^{56}$ | $[-\ln(1-x)]^{2/3}$ | 175.4 | $9.7\times10^{6}$ | $1-(1-x)^{1/2}$ |
| 30% | 1563.1 | $5.3\times10^{66}$ | $[-\ln(1-x)]^{2/3}$ | 194.4 | $1.8\times10^{7}$ | $1-(1-x)^{1/2}$ |
| 60% | 1894.2 | $5.1\times10^{78}$ | $[-\ln(1-x)]^{2/3}$ | 224.8 | $2.5\times10^{8}$ | $1-(1-x)^{1/2}$ |
| 100% | 2047.2 | $2.3\times10^{81}$ | $[-\ln(1-x)]^{2/3}$ | 271.5 | $9.4\times10^{9}$ | $1-(1-x)^{1/3}$ |

**3.3.4 The reaction rate**

Figure 12 shows the variation of reaction rate and temperature with conversion for non-isothermal decomposition of $CaCO_3$ in TGA and MFBRA in $N_2$. The initial decomposition temperature in MFBRA is lower than that in TGA. This is the same as the result shown in Figure11. At the same reaction temperature, the conversion in MFBRA is higher than that in TGA. For example, at 700 °C, the conversion is about 0.04 in TGA, while it is 0.22 in MFBRA. At lower temperatures, the reaction rate is higher for MFBRA than for TGA. When the temperature increases from 700 °C to 800 °C, the conversion increases to 0.47 in TGA and to 0.81 in MFBRA. This means that at higher temperatures the conversion approaches to complete. Therefore, at the same temperature, the reaction rate in MFBRA becomes lower than that in TGA, which is the result of reduced reactant concentration.

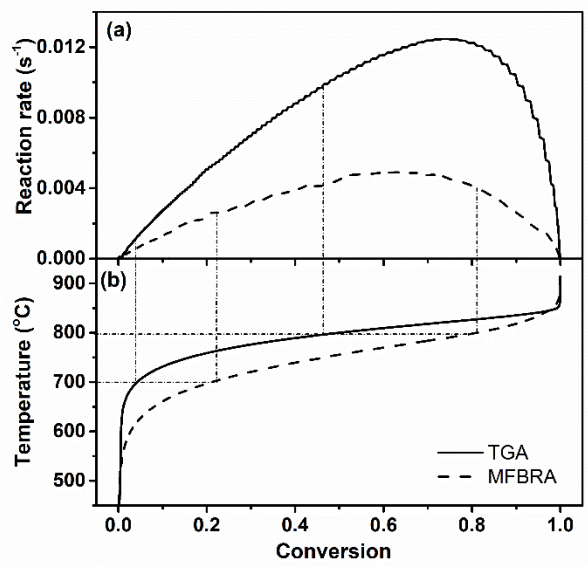


Figure 12. Variations of (a) reaction rate and (b) temperature with conversion at the same heating rate of 40 °C/min in TGA and in MFBRA in $N_2$.

Under the same conversion, the reaction rate in MFBRA is higher than that in TGA under the 100% $CO_2$ environment, as shown in Figure 13. In MFBRA, the reaction rate increases quickly and reaches a maximum at a conversion of about 0.2, then decreased rapidly, while in TGA, the reaction rate changes slowly, and the conversion corresponding to the maximum reaction rate is about 0.5. This again reveals that TGA may mispresent the reaction mechanism because the strong inhibition of external diffusion on reaction, especially when the reaction is carried out in atmosphere of the product gas. On the other hand, MFBRA operates in an environment with gas diffusion essentially eliminated, gas-solid mixing extensively and mass and heat transfer sufficiently high, consequently, the true reaction mechanism can be discovered. Therefore, to obtain intrinsic kinetic parameters of gas-solid reactions, especially in the inhibitory atmosphere of the product gas, MFBRA is certainly advantageous over TGA.

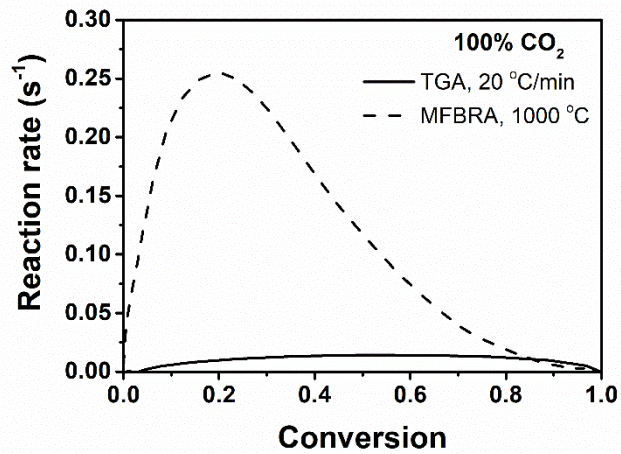


Figure 13. Comparison of reaction rates (a) at the same heating rate of 40 °C/min in $N_2$ and (b) at a heating rate of 20 °C/min in TGA and at 1000 °C in MFBRA in $CO_2$.

## 4. Conclusion

In this study, an isotopes-tagging method was used to permit experiments of reaction kinetics under the inhibitory atmosphere of reaction product gas. The methodology is exemplarily demonstrated by calcination reaction of calcium carbonate under the $CO_2$ containing atmospheres, in which $Ca^{13}CO_3$ was deliberately selected as reactant so that $^{13}CO_2$ produced from calcination reaction becomes easily recognizable because their isotopes are different than those of $^{12}CO_2$ from the atmosphere. The experimental results from both TGA and MFBRA demonstrate that the presence of $CO_2$ in reaction atmosphere has a significant impact on the reaction kinetic parameters such as onset calcination temperature, activation energy and pre-exponential factor. The apparent activation energy increases exponentially with increasing $CO_2$ concentration, but TGA significantly underestimates the reaction rate and overestimates the activation energy due to strong diffusional inhibition by the product gas surrounding the sample crucible. The ratio of the activation energy obtained from TGA to that

obtained from MFBRA is 1.9 in $N_2$, and increase to 3.7 to 8 when $CO_2$ concentration is increased from 1% to 100%. The initial temperatures of $CaCO_3$ decomposition obtained by MFBRA are lower than those obtained by TGA, but very close to the thermal equilibrium predictions. It can be reasonably concluded that for characterizing gas-solid reactions MFBRA is certainly advantageous over TGA, and is quite capable of acquiring real kinetics of reactions carried out in atmosphere of the product gas.

The isotope tagging method is a powerful technology for investigating complex reactions. This study applies it successfully in characterization of a typical reaction that is greatly inhibited by the environment containing the reaction product gas. In the future, it is anticipated that this technology can be continuously developed and applied for investigations of similar reactions.

**Acknowledgments**

The authors gratefully acknowledge the financial support of the National Key R & D Program of China (No. 2018YFF01011400), the National Natural Science Foundation of China (U1908201) and the Natural Science Foundation of Liaoning Province (LJ2020028).

**References**

[1] Bi HT, Ellis N, Abba IA, Grace JR. A state-of-the-art review of gas–solid turbulent fluidization. Chem Eng Sci. 2000; 55(21): 4789-4825.

[2] Shimizu T, Hirama T, Hosoda H, Kitano K, Inagaki M, Tejima K. A twin fluid-bed reactor for removal of $CO_2$ from combustion processes. Chem Eng Res Des. 1999; 77(A1): 62-68.

[3] Harrison DP. Sorption-enhanced hydrogen production: a review. Ind Eng Chem Res. 2008; 47(17): 6486-6501.

[4] Avila I, Crnkovic PM, Milioli FE, Luo KH. Thermal decomposition kinetics of Brazilian limestones: effect of CO2 partial pressure. Environ Technol. 2012; 33(10): 1175-1182.

[5] Martinez I, Grasa G, Murillo R, Arias B, Abanades JC. Kinetics of calcination of partially carbonated particles in a Ca-Looping system for $CO_2$ capture. Energy Fuels. 2012; 26(2): 1432-1440.

[6] Gonzalez B, Grasa GS, Alonso M, Abanades JC. Modeling of the deactivation of CaO in a carbonate loop at high temperatures of calcination. Ind Eng Chem Res. 2008; 47(23): 9256-9262.

[7] Darroudi T, Searcy AW. Effect of $CO_2$ pressure on the rate of decomposition calcite. J Phys Chem. 1981; 85(26): 3971-3974.

[8] Maya JC, Chejne F, Gómez CA, Bhatia SK. Effect of the CaO sintering on the calcination rate of $CaCO_3$ under atmospheres containing $CO_2$. AIChE J. 2018; 64(10): 3638-3648.

[9] Khinast J, Krammer GF, Brunner C, Staudinger G. Decomposition of limestone: The influence of $CO_2$ and particle size on the reaction rate. Chem Eng Sci. 1996; 51(4): 623-634.

[10] Garcia-Labiano F, Abad A, de Diego LF, Gayan P, Adanez J. Calcination of calcium-based sorbents at pressure in a broad range of $CO_2$ concentrations. Chem Eng Sci. 2002; 57(13): 2381-2393.

[11] Jiang W, Hao W, Liu X, Han Z, Yue J, Xu G. Characteristic and kinetics of light calcination of magnesite in micro fluidized bed reaction analyzer. CIESC Journal. 2019; 70(8): 2928-2937.

[12] Yu J, Zeng X, Zhang J, Zhong M, Zhang G, Wang Y, Xu G. Isothermal differential characteristics of gas–solid reaction in micro-fluidized bed reactor. Fuel. 2013; 103: 29-36.

[13] Jess A, Andresen A-K. Influence of mass transfer on thermogravimetric analysis of combustion and gasification reactivity of coke. Fuel. 2010; 89(7): 1541-1548.

[14] Mueller A, Haustein HD, Stoesser P, Kreitzberg T, Kneer R, Kolb T. Gasification kinetics of biomass- and fossil-based fuels: comparison study using fluidized bed and thermogravimetric analysis. Energy Fuels. 2015; 29(10): 6717-6723.

[15] Nowak B, Karlstrom O, Backman P, Brink A, Zevenhoven M, Voglsam S, Winter F, Hupa M. Mass transfer limitation in thermogravimetry of biomass gasification. J Therm Anal Calorim. 2013; 111(1): 183-192.

[16] Zheng Y, Song K, Chi B, Zheng C. Decomposition kinetics of $CaCO_3$ in $CO_2$ atmosphere. J Huazhong Univ of Sci Technol (Nature Science). 2007; 35(8): 87-89.

[17] Xu G. Micro fluidized bed reaction kinetics analyzer. the instrument development project of Chinese Academy of Sciences. China. Project number Y2005014. 2005.

[18] Liu X, Xu G, Gao S. Micro fluidized beds: Wall effect and operability. Chem Eng J. 2008; 137(2): 302-307.

[19] Yu J, Zhu J, Yue J, Sun L, Liu X, Xu G. Development and application of micro kinetic analyzer for fluidized bed gas-solid reactions. CIESC Journal. 2009; 60(10): 2669-2674.

[20] Yu J, Yue J, Liu Z, Dong L, Xu G, Zhu J, Duan Z, Sun L. Kinetics and mechanism of solid reactions in a micro fluidized bed reactor. AIChE J. 2010; 56(11): 2905-2912.

[21] Geng S, Han Z, Yue J, Li Y, Zeng X, Lai D, Yu J, Xu G. Conditioning micro fluidized bed for maximal approach of gas plug flow. Chem Eng J. 2018; 351(110-118.

[22] Liu Y, Wang Y, Guo F, Li X, Li T, Guo C, Chang J. Characterization of the gas releasing behaviors of catalytic pyrolysis of rice husk using potassium over a micro-fluidized bed reactor. Energy Convers Manage. 2017; 136(395-403.

[23] Gao W, Farahani MR, Jamil MK, Siddiqui MK, Siddiqui HMA, Imran M, Rezaee-Manesh R. Kinetic modeling of pyrolysis of three Iranian waste oils in a micro-fluidized bed. Petroleum Science and Technology. 2017; 35(2): 183-189.

[24] Y Yu J, Yao C, Zeng X, Geng S, Dong L, Wang Y, Gao S, Xu G. Biomass pyrolysis in a micro-fluidized bed reactor: Characterization and kinetics. Chem Eng J. 2011; 168(2): 839-847.

[25] Wang F, Zeng X, Shao R, Wang Y, Yu J, Xu G. Isothermal gasification of in situ/ex situ coal char with $CO_2$ in a micro fluidized bed reaction analyzer. Energy Fuels. 2015; 29(8): 4795-4802.

[26] Zeng X, Wang F, Wang Y, Li A, Yu J, Xu G. Characterization of char gasification in a micro fluidized bed reaction analyzer. Energy Fuels. 2014; 28(3): 1838-1845.

[27] Fang Y, Luo G, Chen C, Li J, Zhao H, Duan R, Chen L, Li K, Yao H. Combustion kinetics of in-situ char and cold char in micro-fluidized bed. J Combust Sci Technol. 2016; 22(2): 148-154.

[28] Fang Y, Zou R, Luo G, Chen J, Li Z, Mao Z, Zhu X, Peng F, Guo S, Li X, Yao H. Kinetic study on coal char combustion in a micro fluidized bed. Energy Fuels. 2017; 31(3): 3243-3252.

[29] Chen H, Zheng Z, Chen Z, Yu W, Yue J. Multistep reduction kinetics of fine iron ore with carbon monoxide in a micro fluidized bed reaction analyzer. Metall Mater Trans B.

2017; 48(2): 841-852.

[30] Song Y, Wang Y, Yang W, Yao C, Xu G. Reduction of NO over biomass tar in micro-fluidized bed. Fuel Process Technol. 2014; 118: 270-277.

[31] Chen H, Zheng Z, Chen Z, Bi XT. Reduction of hematite (Fe2O3) to metallic iron (Fe) by CO in a micro fluidized bed reaction analyzer: A multistep kinetics study. Powder Technol. 2017; 316: 410-420.

[32] Li J, Liu X, Zhou L, Zhu Q, Li H. A two-stage reduction process for the production of high-purity ultrafine Ni particles in a micro-fluidized bed reactor. Particuology. 2015; 19: 27-34.

[33] Geng S, Han Z, Hu Y, Cui Y, Yue J, Yu J, Xu G. Methane decomposition kinetics over $Fe_2O_3$ catalyst in micro fluidized bed reaction analyzer. Ind Eng Chem Res. 2018; 57(25): 8413-8423.

[34] Guo F, Dong Y, Lv Z, Fan P, Yang S, Dong L. Kinetic behavior of biomass under oxidative atmosphere using a micro-fluidized bed reactor. Energy Convers Manage. 2016; 108: 210-218.

[35] Samih S, Chaouki J. Development of a fluidized bed thermogravimetric analyzer. AIChE J. 2015; 61(1): 84-89.

[36] Saadatkhah N, Carillo Garcia A, Ackermann S, Leclerc P, Latifi M, Samih S, Patience GS, Chaouki J. Experimental methods in chemical engineering: Thermogravimetric analysis—TGA. Can J Chem Eng. 2019; 98(1): 34-43.

[37] Latifi M, Chaouki J. A novel induction heating fluidized bed reactor: Its design and applications in high temperature screening tests with solid feedstocks and prediction of

defluidization state. AIChE J. 2015; 61(5): 1507-1523.

[38] Latifi M, Berruti F, Briens C. A novel fluidized and induction heated microreactor for catalyst testing. AIChE J. 2014; 60(9): 3107-3122.

[39] Happel J. Transient tracing. Chem Eng Sci. 1978; 33(11): 1567.

[40] Happel J, Suzuki I, Kokayeff P, Fthenakis V. Multiple isotope tracing of methanation over nickel catalyst. J Catal. 1980; 65(1): 59-77.

[41] Criado JM, Morales J. Thermal decomposition reactions of solids controlled by diffusion and phase-boundary processes: possible misinterpretation of the mechanism from thermogravimetric data. Thermochim Acta. 1977; 19(3): 305-317.

[42] Criado JM, Ortega A, Gotor F. Correlation between the shape of controlled-rate thermal analysis curves and the kinetics of solid-state reactions. Thermochim Acta. 1990; 157(1): 171-179.

[43] Criado JM, Ortega A. Remarks on the discrimination of the kinetics of solid-state reactions from a single non-isothermal trace. Therm Anal. 1984; 29(6): 1225-1236.

[44] Vyazovkin S, Wight CA. Kinetics in solids. Annu Rev Phys Chem. 1997; 48: 125-149.

[45] Lu S, Wu S. Advances in calcium carbonate thermal decomposition. CIESC Journal. 2015; 66(8): 2895-2902.